

Global bifurcations and the appearance of a one-dimensional spiral wave in excitable media

Eric N. Cytrynbaum

Department of Mathematics
University of British Columbia

Vancouver, British Columbia, Canada

Timothy J. Lewis

Department of Mathematics
University of California, Davis

California, USA

April 24, 2008

Abstract

It is well known that excitable media can sustain “fast” stable traveling pulses of excitation. In models for which analysis is tractable, the fast pulse solution is known to appear through a saddle-node bifurcation accompanied by a “slow” unstable traveling pulse. Furthermore, the uniform rest state is also a stable solution. It is generally assumed that the boundary between the basins of attractions of the rest state and fast pulse (i.e. threshold) consists of the stable manifold of the slow pulse. We use numerical experiments to explore this issue. Our results indicate that, near the saddle-node bifurcation, the stable manifold of the slow pulse does indeed act as the threshold between the rest state and fast pulse. However, further away from the saddle-node bifurcation, a global bifurcation involving the heteroclinic connections between slow and fast pulses occurs. This bifurcation gives rise to an unstable periodic solution that has been referred to as a one-dimensional spiral wave. Beyond the bifurcation point, the stable manifold of the one-dimensional spiral wave appears to act as the threshold between the rest state and fast pulse.

1 Introduction

Spatially distributed excitable media are ubiquitous in nature, appearing in many chemical, physical and biological systems. These systems have a stable uniform “rest” state, but when perturbed locally above a threshold, they have the ability to generate pulses of elevated activity that propagate without damping (see [22]). Detailed information about the threshold separating the rest state from propagated pulses can be extremely important. For example, it could lead to a better understanding of how aberrant propagated activity can arise in cardiac tissue and induce dangerous arrhythmias [45, 46, 42, 47]. It could also lead to insight into optimal stimuli for annihilating this pathological activity [15, 41, 27, 43, 25]. In this manuscript, we explore the structure of the threshold surface between the basins of attraction of the stable rest state and a stable propagated pulse in an idealized model of excitable media.

1.1 The FitzHugh-Nagumo Equations

The general FitzHugh-Nagumo (FHN) system is a family of two-variable models that capture the essential properties of spatially distributed excitable media and serve as minimal models for excitable systems. The original FitzHugh-Nagumo system [11, 37] was formulated as a reduction of the Hodgkin-Huxley model for nerve axon [18]. Since then, many variants of the general FHN model have been proposed. Some of these models were motivated by specific physiological systems, e.g. the ionic-current based Morris-Lecar model [32]; others were proposed for the sake of analytical tractability, e.g. the piecewise linear McKean and Pushchino models [30, 35]. In their general form, the FHN equations are

$$\begin{aligned}\frac{\partial u}{\partial t} &= D\nabla^2 u + f(u, v) \\ \frac{\partial v}{\partial t} &= \epsilon g(u, v)\end{aligned}\tag{1}$$

where u is the excitation or activator variable, and v is the recovery or inhibitor variable. For typical parameter sets, $f(u, v)$ has three zeros as a function of u over a finite interval of fixed values of v and $\frac{\partial f}{\partial u}(u, v) < 0$ at the lower and upper zeros giving the u equation a bistable structure on that interval. Outside that interval of v , $f(u, v)$ has only one zero. $g(u, v)$ is an increasing function of u and decreasing in v so that the kinetic (spatially homogeneous) equations have only one stable steady state which sits on the

lowest solution branch of the curve $f(u, v) = 0$. The phase plane for one example of such a system is shown in Figure 1 (bottom half of the inset). We consider dynamics in one spatial dimension with diffusive coupling in the excitation variable u only. We concentrate on the case of a spatially periodic domain (i.e., a ring), but we will also consider an infinite domain when appropriate.

1.2 Steady traveling solutions

Three solutions to the FHN system are well-known and well-characterized: (i) the spatially uniform stable rest state, i.e. the solution to $f(u, v) = g(u, v) = 0$, (ii) a fast-moving and generally stable traveling pulse, and (iii) a slow-moving unstable traveling pulse [33, 12, 38, 21] (see Figure 1). For the periodic domain, these traveling pulse solutions correspond to activity circulating around a ring with a fixed velocity. Composite solutions consisting of multiple traveling pulses are also possible.

The level of excitability of the FHN system is dependent on the parameter ϵ : smaller values of ϵ correspond to dynamics with stronger excitability. The stable rest state exists for all positive ϵ , whereas the fast and slow traveling pulse solutions only exist for positive values of ϵ below a critical value ϵ_{SNB} . These traveling pulses disappear via a saddle-node bifurcation as ϵ is increased through ϵ_{SNB} [38] (Figure 1). The terms “fast” and “slow” arise from the observation that the speed of the fast pulse is asymptotically $O(1)$ with respect to ϵ [17, 5], while the speed of the slow pulse is $O(\sqrt{\epsilon})$ [17, 6, 14]. In the singular limit ($\epsilon \rightarrow 0$), the fast pulse can be calculated as a composite structure formed by matched asymptotics of solutions to the singular inner and outer equations [5, 44, 7], and the slow pulse approaches a standing pulse solution to the inner (u) equation of system (1) with v set to the kinetic steady-state constant value [14]. The reduced system, consisting of the inner equation with fixed v , is often referred to as the Nagumo equation [33].

1.3 Threshold solutions

Thresholds that separate two stable states are usually associated with saddle solutions. The unstable manifold of the saddle solution forms heteroclinic connections with the two stable states, and the stable manifold of the saddle solution forms the boundary

(separatrix) between the basins of attraction of the two states. Thus, the stable manifold of the saddle solution acts as a threshold surface between the states. We refer to the stable manifold of the saddle solution as the “threshold” and the saddle solution itself as the “threshold solution”.

For the FHN system, it is generally assumed that the slow pulse is the threshold solution between the rest state and the fast pulse. This should indeed be the case for values of ϵ close to the saddle-node bifurcation at ϵ_{SNB} . For $\epsilon > \epsilon_{SNB}$, the rest state is globally attracting, whereas for $\epsilon < \epsilon_{SNB}$, both the rest state and the fast pulse are presumably stable. Consistent with the structure of a saddle-node bifurcation, we infer that the slow pulse is a saddle solution with one unstable mode for values of ϵ near ϵ_{SNB} . The one-dimensional unstable manifold of the slow pulse is comprised of heteroclinic connections between the slow pulse and the stable rest state and between the slow pulse and the fast pulse. The stable manifold of the slow pulse in turn acts as a threshold surface between the uniform rest state and the fast pulse. Thus, the slow pulse is the threshold solution. Based on the symmetry of the system, the entire structure described above actually appears twice in the phase space, corresponding to both left and right directions of travel.

For small ϵ , there seems to be a fundamentally different scenario. The standing pulse of the Nagumo equation, which is the asymptotic limit of the slow pulse in the singular limit $\epsilon \rightarrow 0$, is known to have a saddle structure with one unstable mode [13]; the stable manifold of the standing pulse is the threshold surface between the stable rest state and the excited state [13, 31, 34]. Furthermore, for ϵ small, the slow pulse for the FHN equations also has a saddle-structure with one unstable mode [14]. However, this does not imply that the slow pulse lies on the threshold surface between rest and the corresponding fast pulse. Small excitatory perturbations of the standing pulse in the Nagumo equation evolve into not one wavefront but two counter-propagating wavefronts [10]. When incorporated into a matched asymptotic analysis, this implies that, for ϵ small, perturbations to the slow pulse should lead either directly to the rest state or to two counter-propagating fast pulses rather than a single fast pulse. On a ring, the two counter-propagating fast pulses would eventually collide and annihilate one another, leading the solution to the rest state. As there is only one unstable mode for ϵ small [14], this observation indicates that the slow pulse is *not* on the threshold

surface between the rest state and the fast pulse but instead lies completely within the basin of attraction of the rest state. On an infinite domain, the slow pulse appears to lie on the threshold between the rest state and the composite solution of two fast pulses propagating indefinitely in opposite directions.

To summarize, although one half of the unstable manifold of the slow pulse always leads to excitation, the details of the long-term behavior appear to be fundamentally different at opposite ends of the ϵ interval for which traveling pulses exist. Near the saddle-node bifurcation, small perturbations to a slow pulse lead either to rest or to a single fast pulse, and the slow pulse is the threshold solution. For small ϵ , small perturbations to a slow pulse lead either to rest or to two counter-propagating pulses and ultimately to rest for the case of a periodic domain. Thus, for ϵ below a critical value, the threshold solution must be something other than the slow pulse. This critical value is the point at which the global bifurcation, which is the main focus of this paper, occurs.

1.4 Outline

Here, we carry out a series of numerical experiments to examine the changes in threshold structure of the FHN system. First, we use a shooting method to explore the long-term behavior of the slow pulse (i.e. dynamics along its unstable manifold). As predicted, there is a fundamental change in this behavior at a critical value $\epsilon = \epsilon^*$. For $\epsilon > \epsilon^*$, suprathreshold perturbations to the slow pulse lead to a single fast pulse; for $\epsilon < \epsilon^*$, suprathreshold perturbations to the slow pulse lead to two counter-propagating fast pulses. Next, we use a second shooting method to directly examine the threshold between the rest state and the fast pulse for the periodic domain. Consistent with the first study, within the numerical accuracy of the technique, we find that for $\epsilon > \epsilon^*$, the threshold solution is indeed the slow pulse. However, for $\epsilon < \epsilon^*$, the threshold between rest and the fast pulse is not the slow pulse but is instead an unstable solution akin to a one-dimensional transect of a spiral wave, which has been referred to as a 1-D spiral wave [26, 9, 28]. Finally, we describe the global bifurcation through which the unstable manifold of the slow pulse redirects itself from single fast-pulse to double fast-pulse and, simultaneously (or nearly so), through which the 1D spiral wave appears.

2 Technical details

The calculations presented throughout this paper are carried out using Morris-Lecar local dynamics on a periodic domain (see Appendix; parameters as given in Table 1). As the domain is much larger than the space scale associated with individual pulses, we assume the observed dynamics are representative of those of the infinite-domain case as well, with the sole exception of pulse collisions due to the periodicity of the domain. With this in mind, we use *leftward* and *rightward* propagation to refer to *clockwise* and *counterclockwise* propagation respectively.

To aid in the description of activity composed of multiple pulses, we introduce the following notation. A rightward propagating fast pulse is denoted as F and a leftward propagating fast pulse by f . Similarly, rightward and leftward propagating slow pulses are referred to as S and s , respectively. The uniform rest state is denoted by R .

Multi-pulse activity composed of several pulses can be described by sequences of these letters that list the pulses in the order of their appearance along the spatial domain. For example, on the infinite domain, fFF would denote, listing from $x = -\infty$ to $x = \infty$, one fast pulse moving leftward, and two fast pulses moving rightward. Although such a solution is not a steady-state-traveling solution because the distances between pulses are time-dependent, it is nonetheless a steady behavior in the more general sense that all three pulses continue to propagate for all time with preserved sequence fFF . In contrast, a sequence of pulses FfF is not steady and converges to F after the collision of the f and leftmost F . On a periodic domain, any sequence of pulses eventually converges to F^n , f^n or the rest solution as determined by the winding number of the initial condition in the phase plane [24, 23]. Note that the maximum power n is determined by the size of the ring and the dispersion curve for the fast pulse (see [22] for a discussion of dispersion curves for FHN). We make the further assumption that convergence properties of single pulses are preserved in the presence of other pulses. For example, if a perturbation to s drives it to f , then an analogous perturbation to sF drives it to fF .

As we are interested in threshold behavior, we define the following terminology which will be useful throughout the rest of this paper:

- R/E threshold – the set of initial conditions which lie on the boundary between

initial conditions that converge to rest without any form of propagated excitation and initial conditions that lead to some form of propagated excitation (possibly transient due to collision on a periodic domain).

- R/E threshold solution – the solution to which initial conditions on the R/E threshold converge.
- R/F threshold – the set of initial conditions which lie on the boundary between initial conditions that ultimately converge to rest and initial conditions that ultimately converge to the single fast pulse solution.
- R/F threshold solution – the solution to which initial conditions on the R/F threshold converge.

3 Threshold and the long-term behavior of the slow pulse

In this section, we describe a numerical shooting method used to examine the R/E threshold, i.e. the threshold between the rest state R and *any significant* suprathreshold activity. We are concerned with any suprathreshold activity whether sustained or transient so, for example, an fF solution on a periodic domain would count as suprathreshold despite its ultimate convergence to rest.

The shooting method involves a search through a one-parameter family of initial conditions and is designed to converge to initial conditions that lie on the R/E threshold surface. At advanced stages of the shooting method, we are thus able to observe (i) the approach to the threshold solution along its stable manifold, (ii) the divergence from the threshold solution along its unstable manifold, and (iii) the subsequent long-term evolution to the rest state R or to suprathreshold activity. As expected, the slow pulse S appears to be the R/E threshold solution for all values of $\epsilon < \epsilon_{SNB}$. However, the long-term behavior of the slow pulse depends on the value of ϵ , with a qualitative change at a critical value of ϵ which we define as ϵ^* .

3.1 The R/E -threshold shooting method

The shooting method consists of a series of simulations of the FHN equations (1), using “square pulse” initial conditions: $u(x, 0) = AP(x, x_1, x_2)$ and $v(x, 0) = v_0P(x, x_3, x_4)$, where $x_3 < x_1 < x_4 < x_2$ and P is a plateau function defined in terms of Heaviside functions $P(y, y_1, y_2) = H(y - y_1)H(y_2 - y)$ (see Figure 2 panel B0). The parameter v_0 and x_1, x_2, x_3, x_4 are set appropriately so that *initial* leftward propagation is prevented. For sufficiently large A , a single rightward propagating fast pulse F is generated. On the other hand, when $A = 0$, the solution converges to rest R . Thus, a shooting method that systematically varies the parameter A can be used to approach initial conditions that lie on the threshold surface between the rest state R and suprathreshold propagated activity.

From iteration to iteration of the shooting method, the value of A is changed as follows. Initially, A_{min} and A_{max} are chosen so that the solution converges to a rightward fast pulse (F) for $A = A_{max}$ and the solution converges to rest (R) for $A = A_{min}$. Simulations are then run with an intermediate value of $A = (A_{min} + A_{max})/2$.

If at any time, $\max_x u(x, t)$ drops below a value just above the resting value of u , the simulation is halted and A_{min} is reset to the current value of A . On the other hand, if $\max_x u(x, t)$ rises above a value just below the peak u value in the fast pulse, the simulation is halted, and A_{max} is reset to the current value of A . A new intermediate value of A is then used in the initial condition for the subsequent simulation. This procedure is iterated until A_{min} and A_{max} are indistinguishable in double precision. This final value of A is used as an approximation of A_{RE} , the critical value of A for which the initial conditions lie on the R/E -threshold surface. The shooting method is carried out for a sequence of ϵ values ranging from 0.04 to 0.40 in increments of 0.02; this provides a broad perspective on near-critical behavior (see Figure 2). Additional simulations are carried out for ϵ between 0.28 and 0.29 in increments of 0.001 to narrow down the bounds on the value of ϵ^* .

To determine when solutions approach traveling pulses, the discrete version of the following function is calculated throughout the simulations:

$$d_{tp}(t) = \min_{x_0} (||u(x, t) - u(x - x_0, t - \tau)|| + ||v(x, t) - v(x - x_0, t - \tau)||) + ||u(x, t)||.$$

This is a measure of how close the solution $u(x, t)$ is to an optimal shift in space of $u(x, t - \tau)$ where τ is a fixed time delay. Note that x_0^{\min}/τ provides an estimate of the traveling speed. When the $||u(x, t)||$ term is omitted, $d_{tp}(t)$ should approach zero for a solution converging to any traveling pulse or the uniform rest state. This additional term is introduced to distinguish between convergence to the fast pulse, the slow pulse, and the uniform rest state.

3.2 Results – a change in long-term slow-pulse behavior at ϵ^*

Figure 2 shows intensity plots of $u(x, t)$ at four different values of A during the shooting method, for each of four values of ϵ . The panels within this figure are described throughout the rest this section.

At all values of ϵ , for $0 \leq A < A_{RE}(\epsilon)$, only subthreshold responses are elicited and the system relaxes to the rest state R (panels A3-D3, A4-D4). Furthermore, values of

A slightly below $A_{RE}(\epsilon)$ lead to transient slow pulses S that eventually collapse to rest R (panels A3-D3).

For values of $\epsilon \geq 0.288$, values of $A > A_{RE}(\epsilon)$ produce responses that develop into single fast pulses F (panels C1, C2, D1, D2). For values of A only slightly above the critical value $A_{RE}(\epsilon)$, there are relatively long transients, during which the solution appears to approach the slow pulse S before eventually converging to the single fast pulse F (panels C2, D2).

At values of $\epsilon \leq 0.287$ and A well above $A_{RE}(\epsilon)$, as seen at larger values of ϵ , a single fast pulse F quickly emerges from the initial condition (panels A1, B1). However, for A only slightly above $A_{RE}(\epsilon)$, the slow pulse S again makes a transient appearance but, in this range of ϵ , excitation does not lead to a single fast pulse but instead to a composite solution consisting of two counter-propagating fast pulses fF (panels A2, B2).

The above results indicate that there is a fundamental change in the threshold behavior at a critical value $\epsilon = \epsilon^*$, where $0.287 < \epsilon^* < 0.288$. For $\epsilon > \epsilon^*$, the slow pulse S is both the R/E threshold solution and the R/F threshold solution. For $\epsilon < \epsilon^*$, the slow pulse S is the R/E threshold solution, but it is not the R/F threshold solution; instead, it is the R/Ff threshold solution. This is a particularly important distinction in the case of a periodic domain, where the two fast pulses fF would eventually collide, annihilate one another, with the solution eventually converging to rest. That is, for a periodic domain, both components of the unstable manifold of the slow pulse S are entirely contained within the domain of attraction of the rest state R .

The overall trend in the suprathreshold behavior of the slow pulse for increasing values of ϵ is well illustrated in panels A2-D2. At low values of ϵ , the slow pulse S can blow up into a retrograde and anterograde fast pulse fF . As the value of ϵ approaches ϵ^* , retrograde propagation is gradually inhibited (panel B2) until it is finally cut off altogether above ϵ^* (panel C2). Although we did not verify it numerically, we postulate that at ϵ^* , the slow pulse S grows into a retrograde slow pulse and anterograde fast pulse sF . Of course, this could only happen on the infinite domain. On a periodic domain, a slow and fast pulse would eventually “collide” leading to some other long-term behavior.

To verify that the intensity plots actually correspond to the composite solutions

described here in terms of the fast and slow pulses, $d_{tp}(t)$ for each simulation is plotted in panels A5-D5. Initial transients are followed by an approach either (i) to rest (labeled A4-D4), (ii) to a transient low level (labeled A3-D3) corresponding to the slow pulse S , (iii) to an intermediate level corresponding to the fast pulse F (labeled A1-D1), or (iv) to a transient high level corresponding to a pair of counter-propagating fast pulses (labeled A2, B2). As describe above in the definition of $d_{tp}(t)$, these flat regions indicate that it is in fact meaningful to describe these solutions in terms of the known traveling pulses.

3.3 A qualitative interpretation of the transition at ϵ^* : phase plane and refractory dynamics

This transition in behavior at ϵ^* can be understood in terms of the effect that the slow pulse has on the refractory variable (v). For low values of ϵ , the slow pulse has a relatively small amplitude in u and has an almost negligible effect on the refractory variable as it propagates through a region. Thus, the “back” of the slow pulse in this regime lies relatively low in the v vs u phase plane as depicted in the left panel of Figure 3. Consequently, as the solution diverges from the slow pulse toward excitation, there is no refractory barrier to retrograde propagation. Therefore, both the “front” and the “back” of the slow pulse grow into true fronts (see reference [44] for a detailed discussion of front propagation) and develop into two counter-propagating fast pulses. For larger values of ϵ , i.e. closer to the saddle-node, the slow pulse has a larger amplitude in u and has a more pronounced effect on v (see the right panel of Figure 3). In this case, as the solution diverges from the slow pulse toward excitation, retrograde propagation is no longer possible; the “front” of the slow pulse evolves into a true front, the “back” evolves into a true back, and only a single anterograde fast pulse emerges.

4 Threshold solutions: slow pulses and one-dimensional spiral waves

The numerical experiments in the previous section indicate that the R/F solution on the periodic domain is the slow pulse for $\epsilon^* < \epsilon < \epsilon_{SNB}$. However, for $0 < \epsilon < \epsilon^*$, the unstable manifold of the slow pulse is embedded in the basin of attraction of the rest state. In order to identify the R/F threshold solution that replaces the slow pulse for $\epsilon < \epsilon^*$, we implement a second shooting method. We stress that this shooting method is designed to identify the threshold between the rest state R and the sustained single fast pulse F (i.e. the R/F threshold solution) specifically and not the threshold between the rest state R and any transient supra-threshold activity (i.e. the R/E threshold solution) as in the previous section.

4.1 The R/F -threshold shooting method

To identify the R/F threshold solution, simulations are performed starting with square-pulse initial conditions as described in the previous section. However, the value of the shooting parameter A is updated differently. Initially, we set $A_{min} = 0$ and A_{max} to be sufficiently large so that the solution with $A = A_{max}$ converges to a single rightward propagating fast pulse F . A simulation with an intermediate value of $A = (\frac{3}{4}A_{min} + \frac{1}{4}A_{max})$ is then performed (the asymmetric update accelerates convergence due to asymmetric computation times). At every time step, the solution is compared to both the rest state R and the single fast pulse F . As soon as the l_2 distance between the solution and either of these two steady solutions falls below a small tolerance value, the simulation is terminated and the values of A_{max} or A_{min} are updated appropriately. In the case of convergence to rest R , the value of A_{min} is updated to A ; for convergence to the fast pulse F , the value of A_{max} is updated to A . The new value of A for the next iteration is taken to be the weighted average of A_{max} and A_{min} as defined above. This process is repeated until A_{max} and A_{min} are indistinguishable in double precision. This final value of A is used as an approximation of A_{RF} , the critical value of A for which the initial condition lies on the R/F threshold surface. The shooting method is carried out for the same sequence of ϵ values as was used in the numerical experiments described in Section 3.

4.2 Results – A one-dimensional spiral wave replaces the slow pulse as the R/F threshold solution below the critical value ϵ^*

For $\epsilon^* < \epsilon < \epsilon_{SNB}$, the results for this second shooting method are identical to those obtained with the shooting method from the previous section, i.e. the R/F threshold solution is the slow pulse.

The sequence of images in Figure 4a shows the results of the shooting method for $\epsilon = 0.18$. These results are characteristic for $\epsilon < \epsilon^*$. Simulations with small values of A (e.g. $A = 50$, bottom panel) approach the rest state R and with sufficiently large values of A (e.g. $A = 62.5$, top panel) initiate single fast pulses F . After several iterations of the shooting method (e.g. $A = 53.69$, first panel above A_{RE}), two counter-propagating fast pulses fF transiently arise before the system ultimately returns to the rest state R through pulse collision on the periodic domain. This is the same behavior described in the previous section. However, curious transient spatio-temporal behavior emerges with further iteration of the shooting method. At $A = 54.008923$ (third panel from top), the initial condition elicits a forward-propagating fast pulse and then a retrograde-propagating fast pulse and then, surprisingly, a new forward-propagating fast pulse arises in its refractory wake. This results in a transient fFF , which eventually evolves to a single rotating fast pulse. As the shooting method progresses further, converging towards $A = A_{RF}$ and the corresponding solution on the R/F threshold surface, more and more new pulses appear: retrograde fast pulses produce new anterograde pulses in their wakes, and the new anterograde pulses produce new retrograde pulses in their wakes. In each case, the process repeats until the activity completely dies out or a single fast pulse F is left. When the total number of pulses generated is even (e.g. $ffFF$), the system ultimately goes to the rest state R , i.e., all activity circulating around the periodic domain is eventually eliminated due to the pairwise collisions and annihilation of pulses. On the other hand, when the total number of pulses generated is odd (e.g. $ffFFF$), the system evolves to a state with a single rightward-propagating fast pulse F .

Despite these peculiar dynamics, there still appears to be a distinct threshold value $A = A_{RF}$ below which the system evolves to rest R and above which the system

evolves to a single rightward-propagating fast pulse F . As A approaches A_{RF} , the total number of pulses increases in a distinctive order. When A is increased toward A_{RF} from below, the number of pulses appears to run through a sequence of even integers $\{0, 2, 4, 6, \dots, 2n, \dots\}$. When A is decreased toward A_{RF} from above, the number of new pulses appears to run through a sequence of odd integers $\{1, 3, 5, 7, \dots, 2n + 1, \dots\}$. $A = A_{RF}$, which yields initial conditions exactly on the boundary between the basins of attraction of the rightward-propagating fast pulse F and the rest state R (i.e. the R/F threshold surface), appears to be an accumulation point for which infinitely many pulses are generated.

In summary, as A increases, we infer that the full sequence of transient pulse trains generated is

$$R, fF, ffFF, \dots, f^n F^n, \dots, f^\infty F^\infty, \dots, f^n F^{n+1}, \dots, fFF, F. \quad (2)$$

On a periodic domain, counter-propagating pulses eventually collide so that even sequences settle down to rest and odd sequences converge to the fast pulse F . The R/F -threshold solution itself, corresponding to $f^\infty F^\infty$ appears to be an oscillation consisting of a sequence of $n, n + 1, n + 2$, and n fast pulses in succession as retrograde and anterograde fast pulses appear one at a time and then a pair of pulses collide on the far side of the domain. The number n is determined by the frequency of the pulse generation, the size of the domain and the dispersion curve for the fast pulse.

On the infinite domain, the solution corresponding to $f^\infty F^\infty$ cannot properly be interpreted as the R/F -threshold solution because, in this regime, there are an infinite number of intervening steady solutions between the basins, i.e. the sequence listed above. This arises from the lack of collisions that occur on the periodic domain.

The above observations suggest that, for $\epsilon < \epsilon^*$, the R/F threshold solution is an unstable periodic solution consisting of a pulse-generating region that alternately sheds retrograde and anterograde pulses. Furthermore, this periodic orbit must be a saddle structure with a single unstable mode because it can be found using a single-parameter shooting method. As mentioned above, initial conditions exactly on its stable manifold (i.e. the R/F threshold surface) would produce sustained periodic activity. As the initial conditions get closer to the threshold surface, more and more cycles are seen as the solution winds away from the unstable periodic solution, generating the sequence

of pulses before ultimately approaching either the single fast pulse or the uniform rest state.

This type of periodic solution is reminiscent of spiral waves in two-spatial dimensions, and thus it has been referred to as a one-dimensional (1-D) spiral wave [26, 8, 9, 28]. The same sequence of transient behavior described above has been observed in one-dimensional excitable media with a local inhomogeneity [9, 28], and a 1-D spiral wave was postulated to be the underlying mechanism. In fact, Ermentrout and Rinzel [9] conjectured that such the 1-D spiral structure could exist in homogeneous excitable media and numerically demonstrated its existence in a linear array of six “cells”. To our knowledge, our work is the first direct evidence for the existence of the 1-D spiral wave in the full homogeneous PDE model.

4.3 Transition at ϵ^* and the link between the slow pulse and the 1-D spiral wave

Figure 5 provides a summary of the results of the search for the R/F threshold solution along with the excitation (R/E) threshold results from Section 3. The black dashed curve $A_{RE}(\epsilon)$ lies along the set of initial conditions that converge to the slow pulse. The red curve $A_{RF}(\epsilon)$ represents the set of initial conditions that converge to the R/F threshold solution. At and above $\epsilon = 0.29$, these two curves are indistinguishable. We note that, for $\epsilon = 0.288$ and $\epsilon = 0.289$, the nature of the threshold solution found using the shooting method could not be clearly distinguished due to numerical limitations. This regime just above ϵ^* is addressed at the end of this section. Below ϵ^* , the R/F threshold solution appears to be a one-dimensional spiral wave.

These results clarify that there are two qualitatively different threshold solutions on either side of ϵ^* , which raises the issue of the nature of the transition at ϵ^* . As ϵ approaches ϵ^* from below, the period of the unstable 1-D spiral appears to increase as longer delays are seen between successive fast pulse initiations (See Figure 6a). Also, fewer fast pulses were seen numerically at the end of the shooting method. This is likely to be due to the fact that the period of the unstable 1-D spiral wave becomes long compared to the time scale at which the solution diverges from the 1-D spiral and the R/F threshold surface.

Interestingly, just below ϵ^* , the activity during the delays between the appearance of successive fast pulses in the 1D spiral resembles the slow pulse. To determine whether the solution is indeed close to the slow pulse, we define the following function that provides a measure of the distance from the slow pulse:

$$d_{sp}(t) = \min_{x_0} (\|u_{sp}(x, t) - u(x - x_0, t)\|_w + \|v_{sp}(x, t) - v(x - x_0, t)\|_w).$$

The “windowed norm” $\|\cdot\|_w$ used to define d_{sp} is the standard l_2 norm but with the integral restricted to the range of x in which the u component of the slow pulse u_{sp} is more than 10% of the maximum amplitude away from its resting value. That is, the integral is taken in a window around the non-resting portion of the slow pulse. Thus, if $d_{sp}(t)$ is close to zero, then on some interval in x , the solution must be close to the slow pulse even if elsewhere on the domain there are large deviations from the slow pulse. The $d_{sp}(t)$ curve calculated for three values of ϵ are plotted in Figure 6e along with space-time intensity plots of the u component of the solution in 6b, c and d.

For $\epsilon = 0.18$ (b), the periodic dips in $d_{sp}(t)$ indicate that there is an interval on which the solution periodically approaches the slow pulse, although the approach is incomplete. For $\epsilon = 0.287$ (c), the solution approaches the slow pulse to a greater degree, which leads to fewer periods of the oscillation being revealed before the shooting method terminates at the double-precision limit. At $\epsilon = 0.35$ (d), the approach appears to be “complete”, as illustrated by the $d_{sp}(t)$ plot. In other words, at this value of ϵ , the boundary solution is actually the slow pulse rather than a solution that periodically comes close to the slow pulse.

4.4 The ambiguous interval near ϵ^*

From the results of the two shooting methods, there is an interval between $\epsilon = 0.287$ and 0.29 in which there appears to be two distinct R/F threshold solutions, the upper one found by the R/F threshold shooting method and the lower found by the R/E threshold shooting method (see Figure 2 panels C2, C3). It is important to note that Figure 5 is not a standard bifurcation diagram because the vertical axis (A) is neither a parameter of the dynamics nor some measure of the amplitude of the solution but rather a representation of a one parameter family of initial conditions. Thus, the disappearance of a particular type of solution does not necessarily indicate

its nonexistence but rather indicates the lack of an initial condition of the form shown in Figure 2 B0 that converges to it. Nonetheless, it seems as though the slow pulse and the 1-D spiral coexist on the boundary in this small interval of ϵ values. However, this could be an artifact of the numerical shooting approach used here. A complete understanding of this region requires a more comprehensive numerical continuation approach.

5 A conjectured global bifurcation of heteroclinic orbits

The observations discussed in previous sections and summarized below, strongly suggest that the appearance of the 1D spiral wave at ϵ^* is fundamentally linked to the change in long-term behavior of the slow pulse:

1. The redirection of the unstable manifold of the slow pulse and the appearance of the 1D spiral wave are apparently coincident with regard to the value of ϵ . As ϵ approaches ϵ^* , the initial conditions that lead to the slow pulse ($A_{RE}(\epsilon^*)$) and the 1D spiral wave ($A_{RF}(\epsilon^*)$) appear to approach each other.
2. The local stability of the slow pulse is not altered at ϵ^* . The stable manifold of the slow pulse appears to remain codimension one, as reflected in the fact that our one-parameter shooting method still converges to it. This rules out the possibility that the 1D spiral wave appears through a local bifurcation of the slow pulse.
3. The period of the 1-D spiral wave increases as ϵ approaches the critical value ϵ^* .
4. The long-term slow-pulse dynamics appears to progress through the following three stages as ϵ increases: (i) for $\epsilon < \epsilon^*$, $S \rightarrow fF$, (ii) for $\epsilon = \epsilon^*$, $S \rightarrow sF$ and (iii) for $\epsilon > \epsilon^*$, $S \rightarrow F$. As ϵ approaches ϵ^* , the 1D spiral wave is characterized by a core that cycles alternately between $S \rightarrow sF$ and $s \rightarrow fS$ which is precisely the critical slow pulse behaviour at ϵ^* .

These observations indicate that the 1D spiral wave appears through a global bifurcation that involves a rearrangement of heteroclinic connections of the unstable manifold of the slow pulse.

To describe the nature of the conjectured bifurcation in more detail, it is convenient to consider the infinite domain rather than the periodic domain. For the infinite domain, counter-propagating pulses do not collide and annihilate one another. Instead, the sets of fast counter-propagating pulses (e.g. fF , fFF , etc.) are attracting invariant solutions, each with its own distinct basin of attraction. The boundaries between these basins consist of the stable manifold of composite solutions that include a slow pulse, e.g. the stable manifold of fSF forms the boundary between fF and fFF .

The full conjectured bifurcation is schematically represented in Figure 7. The stable invariant solutions involving only fast pulses and the rest state are represented by filled

black circles and squares. The unstable invariant solutions that include a slow pulse are indicated as open triangles. The unstable manifolds of the unstable solutions are red curves, and the dashed blue curves represent the stable manifolds, which act as threshold surfaces. The solid green line near the top of each figure represents the family of rightward pulse-like initial conditions; the green shading represents the corresponding family of trajectories evolving from the initial conditions on the solid green line. Note that the diagram only shows activity that begins with a rightward moving pulse. There is a corresponding set of solutions that begin with leftward moving pulses and solutions involving multiple slow pulses, but these are not shown in the diagram. Also note that, although this discussion focuses on the case of an infinite domain, a similar diagram would hold for the periodic domain with the modification that any solution converging to an even number of pulses (black circles) in this diagram would eventually converge to the rest solution R on a periodic domain. Similarly, the basins of attraction of odd numbers of pulses (black squares) would eventually converge to a single fast pulse F .

For ϵ near the saddle node bifurcation at ϵ_{SNB} (Figure 7a), all initial conditions on the solid green line evolve to either the rest state R or the single fast pulse F . The stable manifold of the slow pulse acts as the R/F threshold surface. Although the invariant composite solutions exist, the family of rightward pulse-like initial conditions do not fall into their basins of attraction.

As ϵ gets closer to ϵ^* (Figure 7b), the unstable manifold of S and the stable manifold of Fs (and other pairs of sequentially adjacent unstable solutions) deform and approach one another. This is reflected in Figure 2 panel C2 in which transient retrograde activity appears but quickly dies out. However, the solution space is qualitatively unchanged from Figure 7a.

At ϵ^* (Figure 7c), these manifolds coalesce and form an infinite chain of heteroclinic connections, $S \rightarrow sF \rightarrow fSF \rightarrow fsFF \rightarrow \dots$, i.e. each slow pulse blows up into an anterograde fast pulse and a retrograde slow pulse.

Below ϵ^* (Figure 7d), the heteroclinic connections have completed their rearrangement, creating fundamental changes in the basins of attractions of the stable solutions. The unstable manifold of the slow pulse S now connects to the solution fF , two counter-propagating pulses, and consequently, the stable manifold acts as the threshold between the rest state R and fF . Similarly, the stable manifolds of all composite

solutions with a slow pulse in the middle (e.g. fSF) now act as the threshold surfaces for corresponding stable solutions with approximate slow pulses dying out (e.g. fF) or blowing up into two counter-propagating fast pulses (e.g. $ffFF$). Consequently, the stable manifolds of these unstable invariant solutions are interleaved and divide the family of initial conditions into segments that evolve to all of the different sequences of pulses. Due to the topological constraints of the infinite set of heteroclinic crossings (Figure 7c), a solution consisting of the formation of an infinite number of pulses must exist through the middle of this region (thick black curve in Figure 7d). This solution converges to the 1D spiral. In a more general context, pulse-generating solutions of this type are called “sources” [40].

It is possible that these heteroclinic connections do not form simultaneously at a single value of ϵ but instead occur one by one, most likely from the top down or from the bottom up. The latter case might provide an explanation for the ambiguous interval near ϵ^* mentioned earlier. Provided all connections occur above $\epsilon = 0$, this does not cause fundamental problems for the bifurcation proposed here but simply spreads out the transition across an interval of ϵ values. Due to the minimal interaction between successive pulses along the domain (particularly between a central slow pulse and outward propagating fast pulses), the appearance of these heteroclinic connections are expected to be concentrated in a fairly narrow interval around ϵ^* – recall that we defined ϵ^* to be the value of ϵ at which a heteroclinic connection between S and sF exists. If this is true, only a minimal change in Figure 7 would be necessary.

For the case of a finite periodic domain, the preceding description must be modified in light of the fact that pairs of fast pulses eventually collide with each other on the far side of the domain thereby forming a pulse “sink” [40]. Using the f, s, S, F notation, one analogue of the 1D spiral on a periodic domain, for ϵ close to ϵ^* , would cycle through the *temporal* sequence S, sF, fSF, S, \dots where the first two transitions correspond to movement close to the unstable manifold of S and sF respective while the third corresponds to collision of the f and F pulses. This would be the case on a relative small domain. On a larger periodic domain, the activity associated with the 1D spiral becomes $f^n SF^n, f^n sF^{n+1}, f^{n+1} SF^{n+1}, f^n SF^n, \dots$.

6 Implications of the existence of the 1D spiral wave: reflection and annihilation

Using a set of numerical experiments, we have explored the threshold between the rest state and the traveling fast pulse in a FHN-type model. We find that there is a critical value ϵ^* that separates different types of threshold behavior. For $\epsilon > \epsilon^*$ (lower excitability), the stable manifold of the slow pulse forms the R/E and the R/F threshold surfaces. For $\epsilon < \epsilon^*$ (higher excitability), the slow pulse still acts as the R/E threshold solution. However, between the basins of attraction of the rest state and the single fast pulse, there are a series of regions of initial conditions that lead to solutions consisting of sequences of counter-propagating pulses [9, 28]. At the heart of this series of regions, there is an unstable periodic solution consisting of an infinite sequence of counter-propagating pulses, i.e. the 1D spiral wave [26, 9]. On a periodic domain, the multiple pulse behavior is transient and the 1D spiral wave acts as the threshold solution between the rest state and a circulating fast pulse i.e. the R/F threshold solution.

In our numerical experiments, initial conditions were chosen in a physically unrealistic manner. However, the same dynamics described in this manuscript can arise in physically realistic situations. Structural heterogeneities such as an abrupt increase in cable diameter [9] or a spatially localized decrease in excitability [28] have been shown to uncover the 1D spiral wave. Similarly, the behavior can be uncovered by transient “functional” heterogeneities. Below, we demonstrate this by examining the effects of (i) transient localized increases in refractoriness in front of a fast pulse and (ii) transient localized stimulation in the wake of a fast pulse. The underlying idea is simply that considering a one-parameter family of either stimulus amplitudes or amplitudes of refractory bumps is analogous to consideration of a one-parameter family of initial conditions as studied in previous sections.

Consider a pulse traveling towards a spatially localized region with an elevated refractory level, e.g. resulting from localized “ectopic” activity. In simulations, we have implemented this region by initially setting the recovery variable, v , to have an approximately Gaussian profile with amplitude B and fixed width σ (see Figure 8a). As the pulse approaches the refractory region, the region begins to recover. If the pulse

runs into the region when it has significantly recovered, then the pulse successfully propagates through the region (Figure 8b). If the pulse runs into the region when refractoriness is still high, the pulse dies out and the system goes to rest (Figure 8e). When $\epsilon > \epsilon^*$, there is a sharp boundary in the refractory level set by B between these two behaviors (not shown). However, when $\epsilon < \epsilon^*$ and the 1D spiral wave exists, as the level of refractoriness is altered by changing B , the system exhibits all of the behavior associated with the existence of the 1D spiral (see sequence (2) and Figure 8c). The most robust of this behavior is the successful propagation of the pulse through the refractory region and the generation of a single retrograde or “reflected” pulse (Ff) (Figure 8d). This type of reflected activity has been seen in numerical simulations of models of excitable media [4, 16, 19, 48] and physiological experiments in both cardiac [1, 20, 39] and neural tissue [2, 36], and it has been suggested to underlie the induction of life-threatening cardiac arrhythmias. Analogous behavior in two and three spatial dimensions has been linked to the onset of spiral and scroll waves [28].

As a second example of how the behavior can arise in a physically realistic setting, we consider the effects of a spatially and temporally localized stimulus delivered in the wake of a fast pulse circulating on a periodic domain. This scenario has been studied in the context of both the termination [15] and the onset [46, 42] of cardiac reentrant arrhythmias. We take the stimulus to be a square-wave with amplitude C and fixed small spatial and temporal widths (see Figure 9a). When an appropriately-timed stimulus is delivered in the wake of the pulse, a stimulus of sufficiently large amplitude induces a single retrograde pulse (Figure 9e) [15]. The forward propagating pulse and the new retrograde pulse eventually collide and all activity is annihilated. On the other hand, when the stimulus has a sufficiently small amplitude the rotating fast pulse is phase-reset but survives (Figure 9b). As before, when $\epsilon > \epsilon^*$, a sharp threshold is found between the two behaviors as the amplitude C is increased from zero (not shown). Whereas, when $\epsilon < \epsilon^*$, the system exhibits all of the behavior associated with the existence of the 1D spiral (see sequence (2) and Figure 9c). Thus, stimuli can elicit new supra-threshold activity without necessarily annihilating all activity. Only when an odd number of new traveling pulses are generated is the activity annihilated; this occurs when stimulus amplitudes are greater than the one that produces the 1D spiral wave (see Figure 9d).

In all of the simulations presented in this manuscript, we use the Morris-Lecar (ML) model with all parameters fixed except ϵ (see Table 1). However, we found the same qualitative behavior for the ML model with other parameter sets and for the standard cubic FHN model. Therefore, we expect that the behavior described here is generic for FHN-type models. More work is needed to uncover the details of how parameters affect ϵ^* and the existence of the 1D spiral wave. Furthermore, because of the link between the existence of 1D spiral waves and the induction of cardiac arrhythmias, it is crucial to identify conditions for the existence of a 1D spiral wave and the robustness of its associated transient behavior in physiologically-realistic models (for example, [3, 29]).

7 Appendix

The Morris-Lecar system was first introduced as a physiologically detailed model for barnacle muscle [32]. However, as a model with only two variables, it provides a useful tool for numerical studies of excitable media in general. For such generic studies, it is more common to use the simpler functional forms associated with the proper FitzHugh-Nagumo system which provide analytical tractability. However, the study presented here is a numerical exploration of solutions that lie on boundary of the basins of attraction of two stable solutions and is therefore concerned with solutions that have a saddle structure to them (unstable and stable manifolds). The optimal context for such a study is one in which the positive eigenvalue of the saddle solution is as small as possible thereby ensuring that it can be approached numerically using a shooting technique. Because the saddle solutions (i.e. slow pulse and 1D spiral) necessarily traverse the central region of the phase plane, we conjecture that a parameter range in which this central region has slow dynamics is a convenient one for this study in the sense that the slow pulse is easier to find numerically. In fact, it is unclear whether this conjecture holds up to scrutiny but we use ML dynamics throughout, nonetheless, due to the parametric flexibility it provides in terms of the central region of the phase plane. A more careful study of this conjecture might prove useful in overcoming certain numerical limitations encountered.

The Morris-Lecar system is defined by the following choice of f and g :

$$\begin{aligned} f(u, v) &= -g_{Ca}m_{\infty}(u)(u - E_{Ca}) - g_Kv(u - E_K) - g_l(u - E_l) \\ g(u, v) &= \frac{v_{\infty}(u) - v}{\tau(u)} \end{aligned}$$

where $m_{\infty}(u) = 0.5(1 + \tanh(\frac{u-u_1}{u_2}))$, $v_{\infty}(u) = 0.5(1 + \tanh(\frac{u-u_3}{u_4}))$ and $\tau(u) = 1/\cosh(\frac{u-u_3}{2u_4})$. Parameter values are given in Table 1. For the spatial domain, we consider primarily the case of periodic boundary conditions. The domain size is taken to be unity and we choose a non-dimensional diffusion coefficient sufficiently small to ensure that the domain is not a limiting factor in the propagation of excitation.

Name	Value		Name	Value	
g_l	2	leak conductance	D	0.001	diffusion coefficient
g_K	8.0	K^+ conductance	x_1	0.16	slow pulse u IC parameter
g_{Ca}	4.4	Ca^{2+} conductance	x_2	0.2	slow pulse u IC parameter
u_1	-1.2	$m_\infty(u)$ parameter	x_3	0.13	slow pulse v IC parameter
u_2	18	$m_\infty(u)$ parameter	x_4	0.17	slow pulse v IC parameter
u_3	2	$v_\infty(u), \tau(u)$ parameter	x_0	0.4	stimulus centre
u_4	10	$v_\infty(u), \tau(u)$ parameter	$2w$	0.2	stimulus width
E_l	-60	leak reversal potential	t_{stim}	0.03	stimulus duration
E_K	-84	K^+ reversal potential	τ	0.3	convergence measure delay
E_{Ca}	120	Ca^{2+} reversal potential	dx	0.001	numerical space step
I	10	constant current	dt	0.03	numerical time step

Table 1: Table of parameters used in simulations.

References

- [1] J Antzelevitch, C Jalife, and GK Moe. Characteristics of reflection as a mechanism of reentrant arrhythmias and its relationship to parasystole. *Circulation*, 61:182–191, 1980.
- [2] SA Baccus. Synaptic facilitation by reflected action potentials: Enhancement of transmission when nerve impulses reverse direction at axon branch points. *Proceedings of the National Academy of Sciences*, 95(14):8345–8350, 1998.
- [3] GW Beeler and HJ Reuter. Reconstruction of the action potential of ventricular myocardial fibers. *J. Physiol.*, 268:177–210, 1977.
- [4] C. Cabo and R. C. Barr. Reflection after delayed excitation in a computer model of a single fiber. *Circ. Res.*, 71:260–270, 1992.
- [5] GA Carpenter. A geometric approach to singular perturbation problems with applications to nerve impulse equations. *Journal of Differential Equations*, 23(3):335–367, 1977.

- [6] RG Casten, H Cohen, and PA Lagerstrom. Perturbation analysis of an approximation to the Hodgkin-Huxley theory. *Quarterly of Applied Mathematics*, 32:365–402, 1974.
- [7] E Cytrynbaum and JP Keener. Stability conditions for the traveling pulse: Modifying the restitution hypothesis. *Chaos*, 12(3):788–799, 2002.
- [8] GB Ermentrout and J Rinzel. One-dimensional $\lambda - \omega$ target patterns: empirical stability tests. *Journal of Mathematical Biology*, 10(1):97–100, 1980.
- [9] GB Ermentrout and J Rinzel. Reflected waves in an inhomogeneous excitable media. *SIAM J. Appl. Math.*, 56(4):1107–1128, 1996.
- [10] PC Fife and JB McLeod. The approach of solutions of nonlinear diffusion equations to travelling front solutions. *Archive for Rational Mechanics and Analysis*, 65(4):335–361, 1977.
- [11] R FitzHugh. Impulses and physiological states in theoretical models of nerve membrane. *Biophysical Journal*, 1:445–466, 1961.
- [12] R FitzHugh. Mathematical models of excitation and propagation in nerve. In H. P. Schwan, editor, *Biological Engineering*. McGraw-Hill, Inc., New York, 1969.
- [13] G Flores. The stable manifold of the standing wave of the Nagumo equation. *Journal of Differential Equations*, 80(2):306–314, 1989.
- [14] G Flores. Stability analysis for the slow traveling pulse of the FitzHugh-Nagumo system. *SIAM Journal on Mathematical Analysis*, 22(2):392–399, 1991.
- [15] L Glass and ME Josephson. Resetting and annihilation of reentrant abnormally rapid heartbeat. *Phys Rev Lett*, 75(10):2059–2062, 1995.
- [16] SS Goldstein and W Rall. Changes of action potential shape and velocity for changing core conductor geometry. *Biophys. J.*, 14:731–757, 1974.
- [17] SP Hastings. On the existence of homoclinic and periodic orbits for the Fitzhugh-Nagumo equations. *The Quarterly Journal of Mathematics.*, 27(105):123–134, 1976.
- [18] AL Hodgkin and AF Huxley. A quantitative description of membrane current and its application to conduction and excitation in nerve. *J Physiol*, 117(4):500–544, 1952.

- [19] JF Howe, WH Calvin, and JD Loeser. Impulses reflected from dorsal root ganglia and from focal nerve injuries. *Brain Research*, 116:139–144, 1976.
- [20] J. Jalife and G. K. Moe. Excitation, conduction, and reflection of impulses in isolated bovine and canine Purkinje fibers. *Circ. Res.*, 49:233–247, 1981.
- [21] CKRT Jones. Stability of the traveling wave solution of the FitzHugh-Nagumo system. *Transactions of the American Mathematical Society*, 286(2):431–469, 1984.
- [22] J Keener and J Sneyd. *Mathematical physiology*, volume 8. Springer-Verlag, New York, 1998.
- [23] JP Keener. The topology of defibrillation. *J Theor Biol*, 230(4):459–473, 2004.
- [24] JP Keener and E Cytrynbaum. The effect of spatial scale of resistive inhomogeneity on defibrillation of cardiac tissue. *J Theor Biol*, 223(2):233–248, 2003.
- [25] JP Keener and TJ Lewis. The biphasic mystery: why a biphasic shock is more effective than a monophasic shock for defibrillation. *J Theor Biol*, 200(1):1–17, 1999.
- [26] N Kopell and LN Howard. Target patterns and horseshoes from a perturbed central-force problem: some temporally periodic solutions to reaction-diffusion equations. *Studies in Applied Mathematics*, 64(1):1–56, 1981.
- [27] T Krogh-Madsen and DJ Christini. Resetting and termination of reentry in a loop-and-tail cardiac model. *Phys Rev E Stat Nonlin Soft Matter Phys*, 77(1 Pt 1):011916, 2008.
- [28] TJ Lewis. *The effects of nonexcitable regions on signal propagation in excitable media: propagation failure and reflection*. PhD thesis, University of Utah, 1998.
- [29] CH Luo and Y Rudy. A dynamic model of the cardiac ventricular action potential. i. simulations of ionic currents and concentration changes. *Circ Res*, 74(6):1071–1096, 1994.
- [30] HP McKean. Nagumos equation. *Advances in mathematics*, 4(3):209–&, 1970.
- [31] V Moll and SI Rosencrans. Calculation of the threshold surface for nerve equations. *SIAM J. Appl. Math.*, 50:1419 – 1441, 1990.
- [32] C Morris and H Lecar. Voltage oscillations in the barnacle giant muscle fiber. *Biophys. J.*, 35(1):193–213, 1981.

- [33] JS Nagumo, S Arimoto, and S Yoshizawa. An active pulse transmission line simulating nerve axon. *Proceedings of the Institute of Radio Engineers*, 50:2061–2071, 1962.
- [34] JC Neu, RS Preissig, and W Krassowska. Initiation of propagation in a one-dimensional excitable medium. *Physica D: Nonlinear Phenomena*, 102(3-4):285–299, 1997.
- [35] AM Pertsov, EA Ermakova, and AV Panfilov. Rotating spiral waves in a modified FitzHugh-Nagumo model. *Physica D Nonlinear Phenomena*, 14:117–124, 1984.
- [36] F Ramon, RW Joyner, and JW Moore. Propagation of action potentials in inhomogeneous axon regions. *Federation Proc.*, 34:1357–1363, 1975.
- [37] J Rinzel. Excitation dynamics: insights from simplified membrane models. *Fed Proc*, 44(15):2944–2946, 1985.
- [38] J Rinzel and JB Keller. Traveling wave solutions of a nerve conduction equation. *Biophys J*, 13(12):1313–1337, 1973.
- [39] GJ Rozanski, J Jalife, and GK Moe. Reflected reentry in nonhomogenous ventricular muscle as a mechanism of cardiac arrhythmias. *Circulation*, 69:163–173, 1984.
- [40] Scheel A. Sandstede B. Defects in oscillatory media: Toward a classification. *SIAM J. Appl. Dyn. Sys.*, 3(1):1–68, 2004.
- [41] S Sinha and DJ Christini. Termination of reentry in an inhomogeneous ring of model cardiac cells. *Physical Review E*, 66:061903–1 – 061903–7, 2002.
- [42] CF Starmer, VN Biktashev, DN Romashko, MR Stepanov, ON Makarova, VI Krinsky, , Stepanov M. R. , Makarova O. N, and Krinsky V. I. Vulnerability in homogeneous excitable media: Analytical and numerical studies of unidirectional propagation. *Biophysical J.*, 65:1775–1787, 1993.
- [43] N Trayanova, R Gray, D Bourn, and J Eason. Virtual electrode induced positive and negative graded response: New insights into fibrillation induction and defibrillation. *J. Cardiovasc. Electrophys.*, 14:756 – 763, 2003.
- [44] JJ Tyson and JP Keener. Singular perturbation theory of traveling waves in excitable media (a review). *Physica D*, 32:327–361, 1988.

- [45] AT Winfree. *When Time Breaks Down: The Three-Dimensional Dynamics of Electrochemical Waves and Cardiac Arrhythmias*. Princeton University Press, Princeton, 1987.
- [46] AT Winfree. Electrical instability in cardiac muscle: phase singularities and rotors. *J Theor Biol*, 138(3):353–405, 1989.
- [47] A Xu and MR Guevara. Two forms of spiral-wave reentry in an ionic model of ischemic ventricular myocardium. *Chaos*, 8(1):157–174, 1998.
- [48] Y Zhou and J Bell. Study of propagation along nonuniform excitable fibers. *Math. Biosci.*, 119:169–203, 1994.

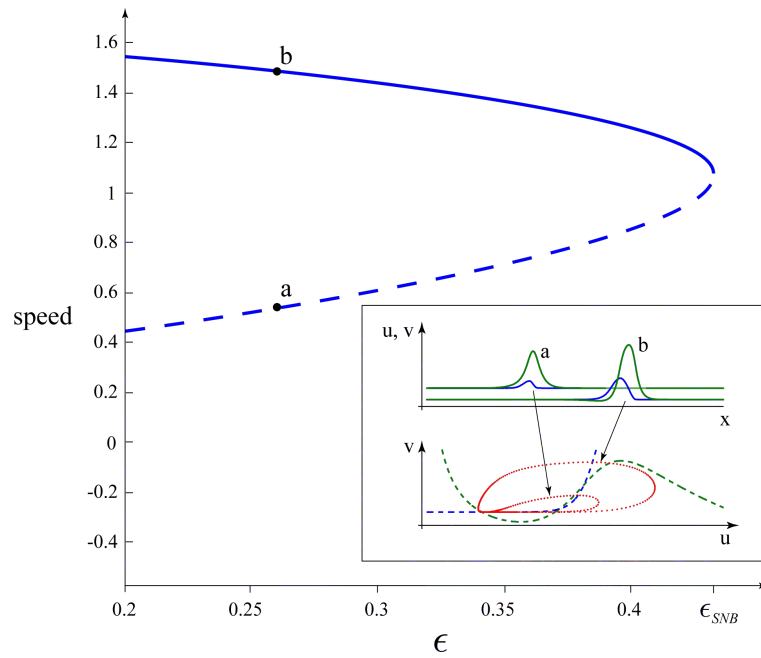


Figure 1: The speeds of slow (dashed) and fast (solid) pulses plotted as functions of ϵ , calculated numerically using a shooting method for the Morris-Lecar system (see appendix and Table 1). A saddle-node bifurcation of the fast and slow pulses occurs near $\epsilon = 0.43$. Examples of slow (a) and fast (b) pulses for $\epsilon = 0.26$ are plotted as function of x and in the phase plane as curves parametrized by x (inset).

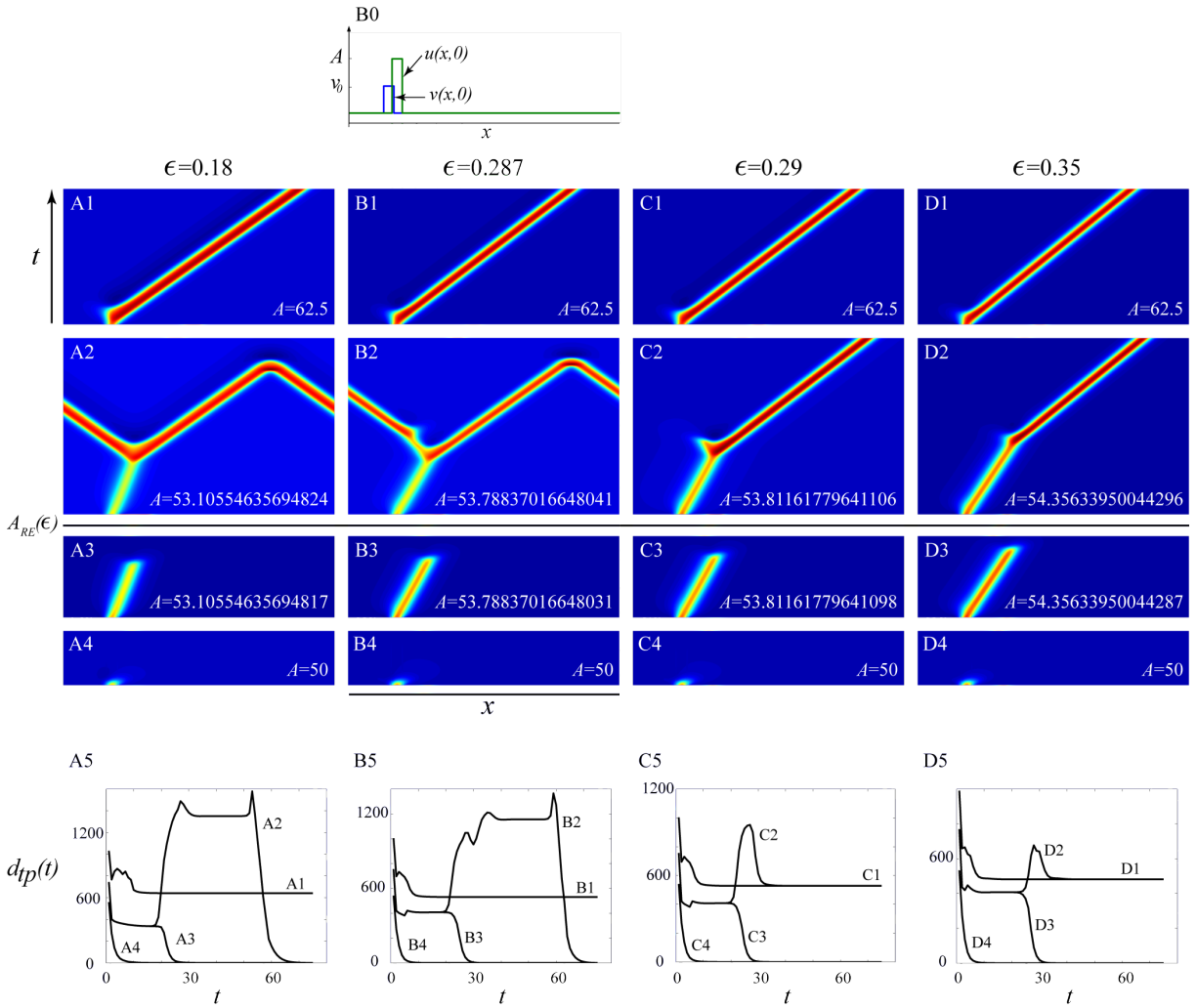


Figure 2: The results of the shooting method used to find the R/E threshold solution at four values of ϵ are shown as intensity images ($u(x,t)$ only). A schematic of the initial condition used in all simulations is shown in panel B0 (top). All parameters are given in Table 1 except for ϵ and A , the amplitude of u in the initial condition, which are specified in the figure for each column and panel, respectively. Panels A1-D1 show direct convergence to the fast pulse for A sufficiently large. Panels A4-D4 show convergence directly to rest for a sufficiently low value of A . Panels A2-D2 and A3-D3 show transient convergence to the slow pulse followed by excitation and convergence to rest, respectively. For $\epsilon < \epsilon^*$ (A2 and B2), excitation consists of two fast pulses but for $\epsilon > \epsilon^*$ (C2 and D2) only one fast pulse emerges. Approaching ϵ^* from below (A2 \rightarrow B2), note that the retrograde fast pulse is gradually pinched down until it finally fails to propagate above ϵ^* (C2). Panels A5-D5 show $d_{tp}(t)$ for each simulation portrayed in the upper panels. Three or four flat regions are evident in each simulation corresponding to the rest state R , the slow pulse S , the fast pulse F and, when present, the double fast pulse fF .

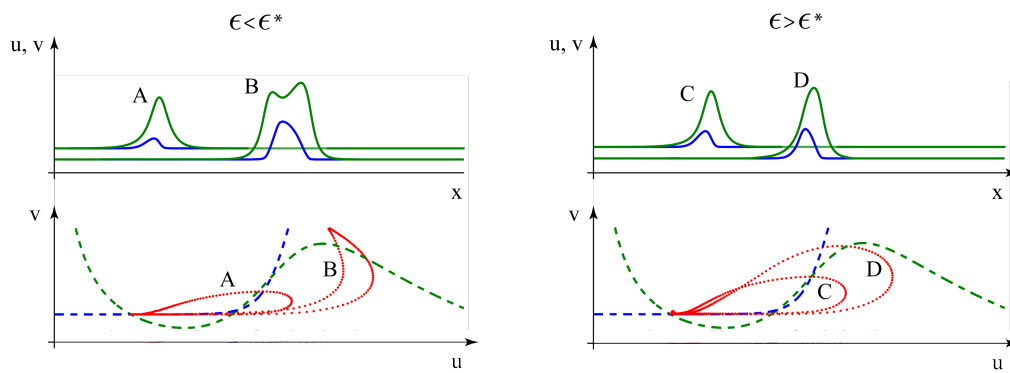


Figure 3: Comparison of slow pulse excitation above and below the critical value of ϵ^* . Solutions $u(x, t), v(x, t)$ are plotted as functions of x (top) and parametrized by x in the $u - v$ phase plane (bottom) at two different points in time, when the solutions are close to the slow pulse (A, C) and during subsequent excitation (B, D). For $\epsilon < \epsilon^*$ (left panel), the “back” of the slow pulse is low in the phase plane and grows into a true front leading to two counter-propagating fast pulses. We use $\epsilon = 0.26$ to illustrate this case. For $\epsilon > \epsilon^*$ (right panel - illustrated with $\epsilon = 0.38$), the “back” of the slow pulse is higher in the phase plane and grows into a true back leading to a single fast pulse.

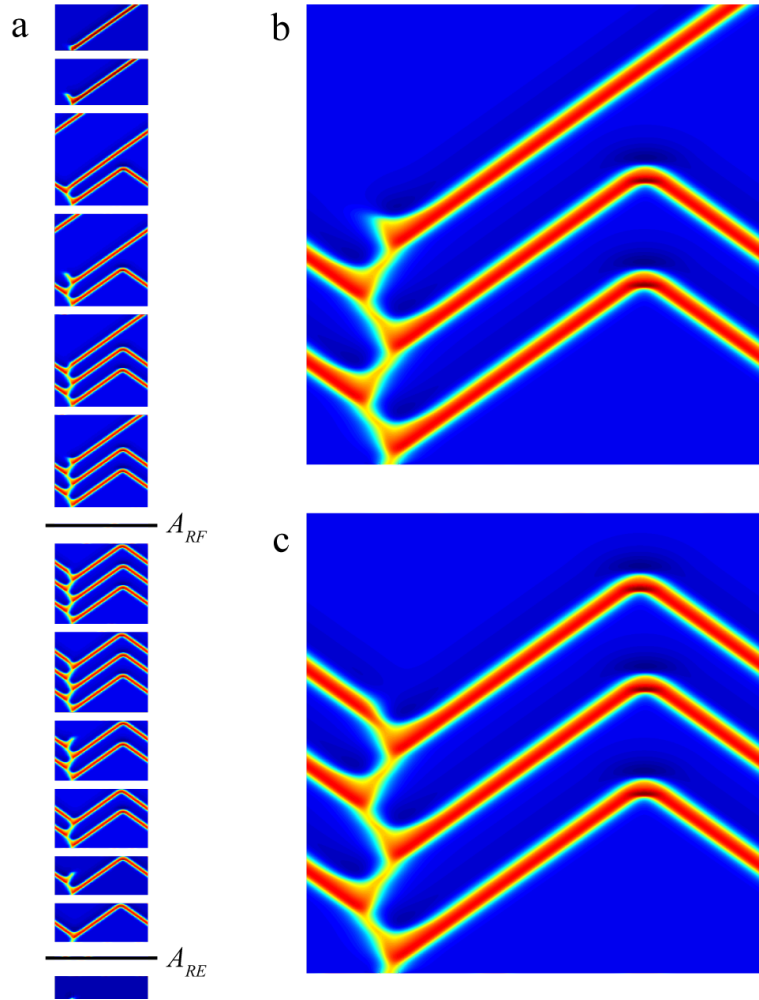


Figure 4: Results of the shooting method used to find the R/F threshold for $\epsilon = 0.18$ (typical of $\epsilon < \epsilon^*$). (a) Space-time plots for a range of values of A used during the shooting method (increasing A from bottom to top, vertical increments not to scale). Below A_{RE} , convergence is directly to rest. Between A_{RE} and A_{RF} , the number of generated pulses increases in pairs giving an even sequence. Notice in the third image from the bottom, excitation of the retrograde pulse is slow enough that a second anterograde fast pulse almost appears (looking briefly like a slow pulse, then dying out). In the fourth image from the bottom, this anterograde excitation succeeds in forming a fast pulse but because $\epsilon < \epsilon^*$ and the transient is close to a slow pulse, a pair of counterpropagating pulses emerges. This is repeated in each pair-adding stage of the sequence. Above A_{RF} the number of generated pulses decreases in pairs through an odd sequence. Magnified versions of the two solutions closest to and on either side of the R/F threshold are shown in (b) (above the R/F threshold) and (c) (below the R/F threshold).

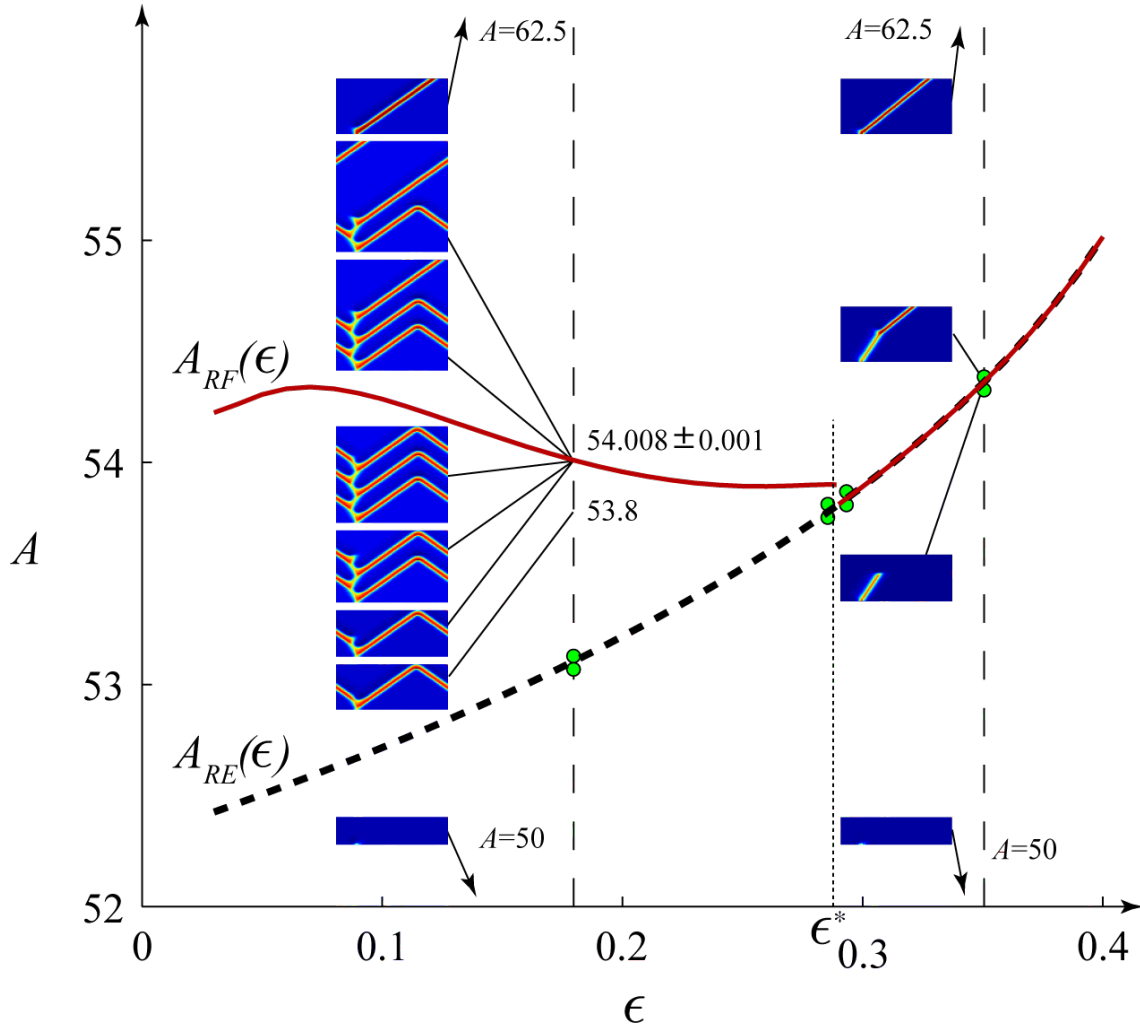


Figure 5: A parameter/initial condition diagram depicting basins of attraction and their boundaries in the $\epsilon - A$ plane. The thick black dashed curve represents initial conditions (ICs) that converge to the slow pulse ($A_{RE}(\epsilon)$). The solid red curve represents the boundary between convergence to rest and convergence to the fast pulse ($A_{RF}(\epsilon)$). To the accuracy of our calculations, above ϵ^* , $A_{RE}(\epsilon)$ and $A_{RF}(\epsilon)$ are indistinguishable. Below ϵ^* , $A_{RE}(\epsilon)$ and $A_{RF}(\epsilon)$ differ, with $A_{RE}(\epsilon)$ corresponding to the slow pulse and $A_{RF}(\epsilon)$ corresponding to the 1-D spiral wave. ICs below $A_{RE}(\epsilon)$ converge directly to rest. ICs above $A_{RE}(\epsilon)$ but below $A_{RF}(\epsilon)$ undergo transient excitation before ultimately converging to rest (on a periodic domain). ICs above $A_{RF}(\epsilon)$ converge to the fast pulse. Example simulations are shown for $\epsilon = 0.18$ and $\epsilon = 0.35$ (vertical thin dashed curves). The $\epsilon = 0.18$ sequence, also shown in more detail in Figure 4, shows the even and odd sequences described in the text – note that the entire even cascade for $n > 2$ exists in a narrow interval near A_{RF} (54.008 ± 0.001). The $\epsilon = 0.35$ sequence appears in Figure 2 panels D1-D4 and is repeated here for context. Simulations from Figure 2 panels A2-D2 and A3-D3 are represented as green dots.

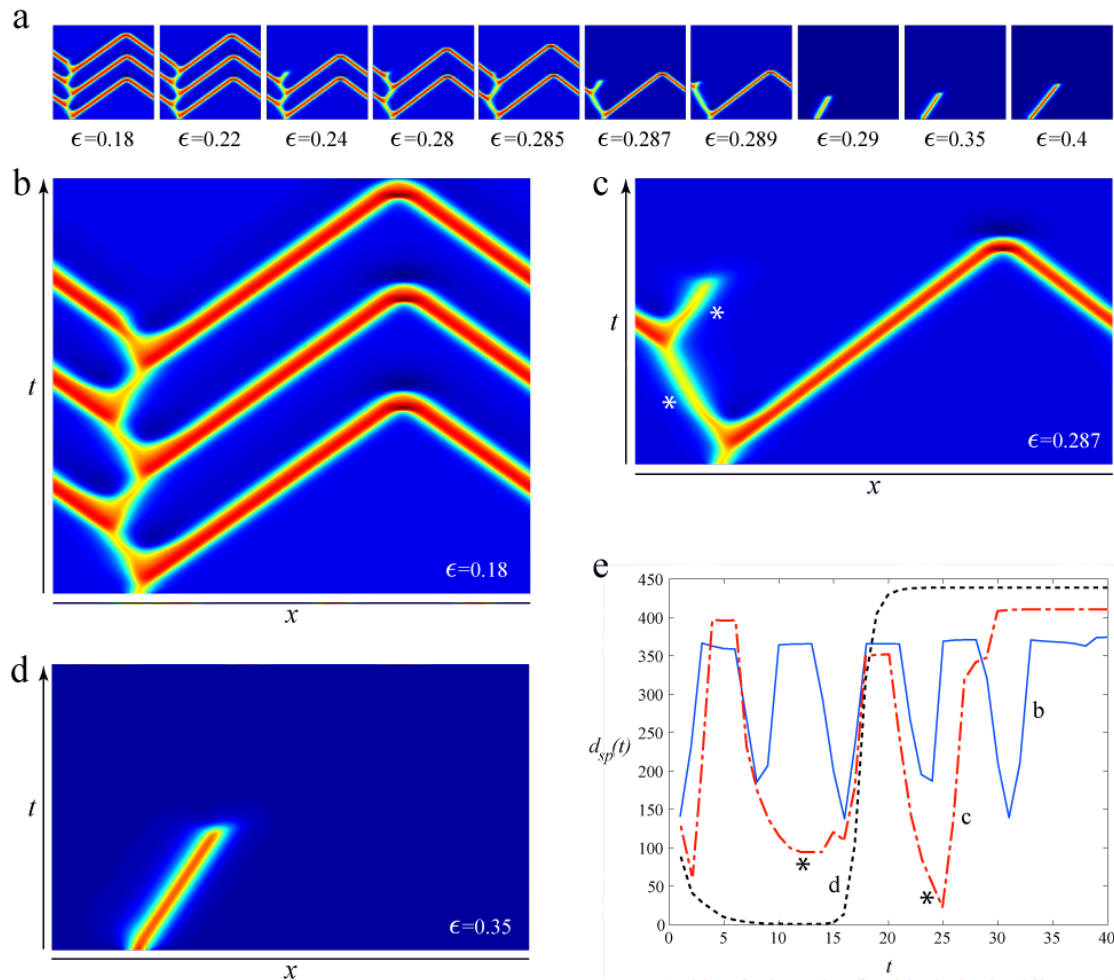


Figure 6: (a) Simulations corresponding to ICs just below $A_{RF}(\epsilon)$ for a selection of ϵ values. Magnifications for $\epsilon = 0.18, 0.287$ and 0.35 are shown in (b), (c) and (d), respectively. (e) The windowed distance from the slow pulse, $d_{sp}(t)$, for each of the highlighted values of ϵ . For $\epsilon = 0.18$ (b- solid blue), a region of the solution periodically approaches the slow pulse (four distinct minima in $d_{sp}(t)$). For $\epsilon = 0.287$ (c- dash-dot red), the solution locally approaches the slow pulse to a greater degree and the period is larger (two minima marked with asterisks corresponding to the two apparent slow pulses also marked with asterisks in (c)). For $\epsilon = 0.35 > \epsilon^*$ (d- dashed black), the approach to the slow pulse is apparently complete and no periodicity is seen. In (a), note that the apparent period increases with increasing ϵ until convergence to the slow pulse occurs at and above $\epsilon = 0.29$.

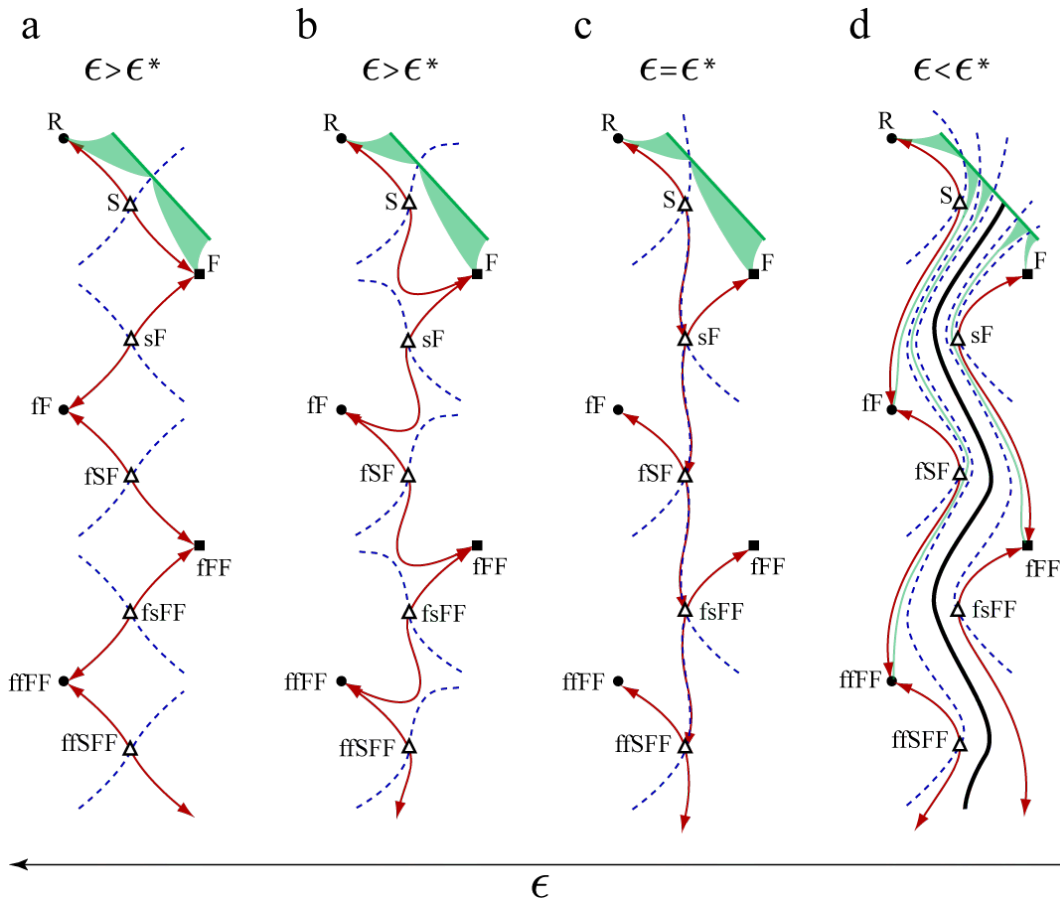


Figure 7: A sequence of cartoon phase portraits illustrating the proposed heteroclinic bifurcation on the infinite domain. Steady traveling pulse solutions and composites solutions are denoted by circles, triangles and squares. The top circle is the rest state. Solid shapes denote stable solutions, empty shapes denote unstable solutions. Red arrows represent the one-dimensional unstable manifolds of the slow pulse and composite solutions involving slow pulses. Blue dashed curves represent codimension-one stable manifolds. The thick black zig-zag solution in (d) converges to the one-dimensional spiral wave. ϵ decreases from left to right. In (a) and (b), the slow pulse is the R/F threshold solution and its stable manifold is the threshold surface. The dynamics at the proposed bifurcation point are illustrated in (c). For $\epsilon < \epsilon^*$ (d), the R/F threshold consists of the entire region between the stable manifolds of S and sF . On a finite periodic domain, all solutions to the left of the thick black zig-zag curve, other than the dashed blue curves, converge to rest and the dashed blue curves converge to the slow pulse S . All solutions to the right of the thick black zig-zag curve, other than the dashed blue curves, converge to the fast pulse F . The long-term behavior of the dashed blue curves to the right of the zig-zag curve (on a periodic domain) remains an open problem.

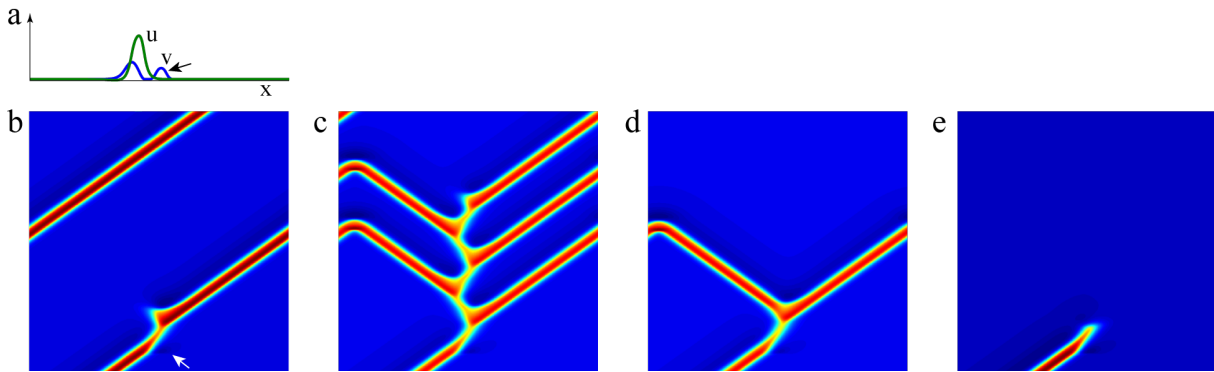


Figure 8: The effects of propagation through a transient refractory region. A refractory bump, in the form of the addition of a Gaussian ($B \exp(-(x - x_0)^2/\sigma^2)$) to the recovery variable v , is placed ahead of fast pulse. This is illustrated in (a) (black arrow) and visible as a slightly darker blue region just in front of the fast pulse in all four images (white arrow in (b)). (b)-(e) show the effect of changing the amplitude B with x_0 fixed and $\sigma = 0.01$ and $\epsilon = 0.18 < \epsilon^*$. (b) For sufficiently small B ($B = 0.1838$), the fast pulse successfully crosses the refractory region. (c) By using a shooting method on B , all of the transient behavior associated with the existence of the 1D spiral can be observed ($B = 0.1838374797093847851092718$). (d) For $B = 0.1839$, the fast pulse successfully crosses the refractory region with a delay and a retrograde fast pulse is produced. (e) For sufficiently large B ($B = 0.1840$), the fast pulse hits the refractory region and dies out.

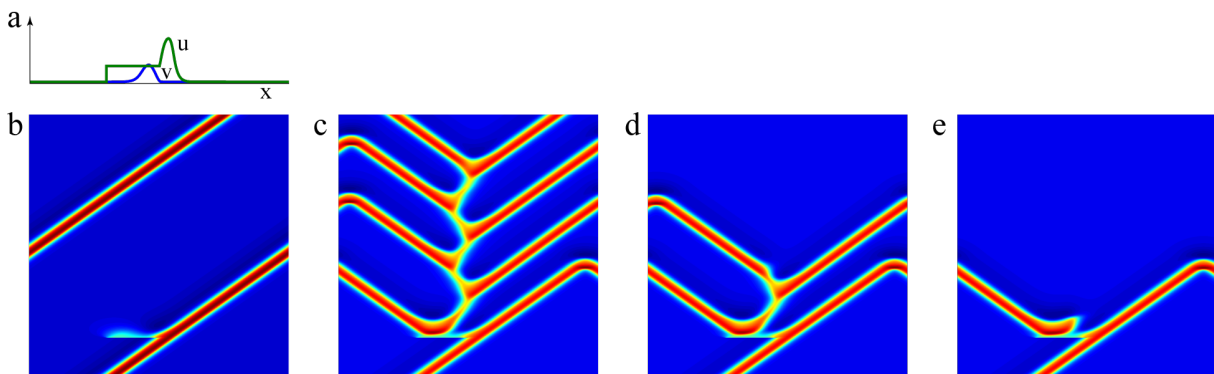


Figure 9: The effects of stimuli in the wake of a fast pulse rotating on a 1D excitable medium. A square-wave stimulus is delivered in the wake of the fast pulse. The stimulus has amplitude C , temporal width $\Delta t = 0.03$ and spatial width $\Delta x = 0.2$ and $\epsilon = 0.18$ is in the sub- ϵ^* range. (b) For sufficiently small C ($C = 1200$), the stimulus has only a subthreshold effect. (c) By adjusting C , all of the transient behavior associated with the existence of the 1D spiral can be observed (image corresponds to $C = 1369.42006681669181$). (d) For $C = 1369.421$, the stimulus elicits a retrograde fast pulse, an anterograde fast pulse and subsequently another retrograde fast pulse with the final result of convergence to rest. (e) For sufficiently large C ($C = 1406.2$), the stimulus elicits only a new retrograde fast pulse, eventually eliminating all activity.